Received: 17 November 2025 | Revised: 4 February 2026 | Accepted: 2 March 2026 | Published online: 15 March 2026

RESEARCH ARTICLE

Artificial Intelligence and Applications
2026, Vol. 00(00) 1–16
DOI: 10.47852/bonviewAIA62028273

BON VIEW PUBLISHING

Adaptive Mechanisms of Foot Function and Control Induced by Dance Training

Xiangli Gao[1,2], Datao Xu[1], Minjun Liang[1], Zanni Zhang[1], Tianle Jie[1,3], Huiyu Zhou[1,4], Jingyi Ye[1,2], Zsolt Radak[2] and Yaodong Gu[1,*]

[1] *Faculty of Sports Science, Ningbo University, China*

[2] *Department of Kinesiology, Hungarian University of Sports Sciences, Hungary*

[3] *Doctoral School on Safety and Security Sciences, Óbuda University, Hungary*

[4] *Zhejiang Engineering Research Center for New Technologies and Applications of Helium-Free Magnetic Resonance Imaging, Ningbo No. 2 Hospital, China*

Abstract: This study explored the adaptive remodeling of the foot's neuro-biomechanical system induced by dance training. A multimodal function-and-control framework was established, integrating kinematic and kinetic analyses, electromyographic synergy modeling, and finite element simulation to reveal adaptive changes from multiple perspectives. The results showed that Latin dancers exhibited greater ankle and metatarsophalangeal flexion angles and joint moments but lower angular velocities during landing, indicating a more efficient energy absorption and release mechanism. Their muscular synergy patterns were activated earlier and in a more compact manner. Finite element analysis revealed higher stress concentrations in the first and second metatarsals and phalanges, suggesting adaptive changes in load transmission. These findings demonstrate that dance training can induce a feedforward-driven, multilevel coupling mechanism that enhances coordination among neural control, mechanical output, and structural remodeling, thereby improving impact absorption and postural stability. This study reveals the hierarchical plasticity of the neuro-biomechanical system during complex skill learning and provides new perspectives for the development of precision training, injury prevention, and rehabilitation strategies.

Keywords: dance training, neuro-biomechanical adaptation, feedforward control, foot biomechanics, non-negative matrix factorization

1. Introduction

Long-term repetitive training can induce profound transformations across multiple human physiological systems. These adaptations encompass not only remodeling of the musculoskeletal framework but also enhancements in motor performance and reorganization of neural control strategies [1, 2]. Rather than representing isolated structural adjustments, such changes reflect coordinated reconstruction across different functional levels. As the interface between the body and the ground, the foot plays a pivotal role in maintaining posture, transmitting mechanical energy, and coordinating movement [3]. It functions both as a structural support and a propulsion mechanism while contributing to balance through proprioceptive and tactile feedback [4, 5].

Latin dance is characterized by frequent forefoot loading, rapid shifts of the center of mass, and multidirectional rotations. Its rhythmical and highly variable movement patterns impose exceptional demands on lower-limb coordination and postural control [6, 7]. Unlike linear or cyclic exercises such as running, the multiaxial and nonlinear nature of Latin dance makes it an ideal paradigm for examining multilevel motor adaptations in humans [8]. Previous research by Stawicki et al. [9] and Virtanen et al. [10] has shown that dancers often outperform non-dancers in both static and dynamic balance and exhibit heightened proprioceptive acuity. These advantages are generally attributed to long-term, high-intensity practice that refines postural control strategies. Dance training has also been linked to improvements in movement accuracy and flexibility of lower-limb coordination [11]. Nevertheless, most studies have focused on isolated parameters, providing limited insight into the interactions among structural, functional, and neural control mechanisms. Studies relying solely on single-modality data—such as kinematic, kinetic, or electromyographic analyses—have yet to fully reveal the multilayered adaptive processes of the foot in complex motor tasks [12, 13].

Our previous work extended beyond examining individual muscle activity by analyzing the synergistic organization of muscle groups, thereby offering a more comprehensive understanding of dancers' neuromuscular control patterns [7, 14]. These findings

***Corresponding author:** Yaodong Gu, Faculty of Sports Science, Ningbo University, China. Email: guyaodong@nbu.edu.cn

suggest that long-term dance training reshapes the temporal organization and mechanical output of the neuromuscular system, enhancing energy efficiency and postural stability. Although existing evidence supports the positive effects of dance training on motor control, integrative studies that combine structural, functional, and neural dimensions remain scarce [15, 16].

Within the human movement chain, the foot serves as a highly integrated node where morphology, function, and neural regulation intersect. Its anatomical configuration determines the pathways of load transmission, its dynamic behavior reflects the efficiency of energy absorption and release, and its neuromuscular coordination maintains inter-joint balance [17, 18]. Thus, the foot can be viewed as a microcosm of the body's adaptive design and a valuable entry point for studying hierarchical motor adaptations. Despite considerable progress in understanding musculoskeletal remodeling, functional optimization, and neural plasticity, the mechanisms underlying how long-term training influences the coordination between foot structure, performance, and neuromuscular regulation remain insufficiently explored.

This gap is particularly evident in dance forms that emphasize forefoot support and rapid weight transfer, where the foot must sustain dynamic equilibrium under frequent loading and complex postural demands [19, 20]. To date, the mechanisms by which multilevel coordination within the foot balances stability and efficiency are poorly defined, and potential trade-offs between enhanced control precision and accumulated mechanical stress have received little attention. Continuous forefoot loading and repeated rotations may contribute to localized stress accumulation [21], yet their relationship to functional optimization remains unclear. To address these challenges, the present study introduces a multimodal analytical framework integrating functional and control coupling. By combining kinematic and kinetic assessments, electromyographic synergy modeling, and finite element (FE) simulations, the study explores the adaptive remodeling of the foot's neuro-biomechanical system resulting from long-term Latin dance training. Through cross-level data integration and correlation analyses, it seeks to elucidate how functional and neural components interact to achieve coordinated optimization during complex motor tasks. Ultimately, this research provides empirical support for theoretical models of motor adaptation and offers practical insights for precision training, injury prevention, and rehabilitation design.

2. Methods

2.1. Participants

Based on the calculation using G*Power 3.1 (with an effect size of 0.9, a significance level of 0.05, and a statistical power of 0.8), a total of 42 female participants were recruited for this study, including 21 in the Latin dancer (LD) group with more than five years of dance experience and a training frequency of at least twice per week and 21 in the non-dancer (ND) group. The demographic characteristics of the LD group were as follows: age = 24.76 ± 1.12 years, height = 164.14 ± 2.92 cm, and body weight = 53.13 ± 2.52 kg. The ND group had a mean age of 23.33 ± 0.94 years, a height of 165.89 ± 2.64 cm, and a body weight of 52.22 ± 2.48 kg [14]. Biomechanical parameters were systematically collected from all participants. For the FE analysis, one representative female LD (26 years old, 163 cm in height, 54 kg in body mass) was selected to ensure that the simulation results accurately reflected the foot mechanical characteristics under dance-specific training conditions. The subject's right foot was identified as having a normal arch, as determined by an arch height index (> 0.356) and a foot posture index ranging from −4 to 4 [22, 23]. A three-dimensional FE model of the right foot was constructed using her CT imaging data. The participant had no history of lower-limb musculoskeletal injuries within the six months preceding the experiment.

2.2. Experimental equipment

In this study, lower-limb kinematics, kinetics, and neuromuscular activity were synchronously collected to investigate foot function and control during a single-leg landing task. A Vicon motion capture system comprising eight infrared cameras (Oxford Metrics Ltd., Oxford, UK) was used to record three-dimensional marker trajectories, while a force platform (Kistler, Switzerland) simultaneously measured ground reaction forces (GRFs). Kinematic data were sampled at 200 Hz, and kinetic data were recorded at 1000 Hz, providing sufficient temporal resolution for dynamic landing analysis [24]. The synchronized kinematic and kinetic data were subsequently used to compute lower-limb joint angles, joint moments, and loading characteristics. To quantify neuromuscular activation patterns, surface electromyography (EMG) signals were collected using a Delsys EMG system (Delsys, Boston, USA) at a sampling rate of 1000 Hz [25]. EMG data were used to characterize muscle activation timing and magnitude during the landing phase, thereby reflecting neuromuscular control strategies. To comprehensively investigate the neuromuscular control of the functional foot complex, 10 muscles associated with foot motion, stability, and arch support were selected: tibialis anterior (TA), tibialis posterior (TP), medial and lateral gastrocnemius (MG, LG), peroneus longus and brevis (PL, PB), flexor digitorum longus (FDL), extensor digitorum longus (EDL), flexor hallucis longus (FHL), and extensor hallucis longus (EHL). These muscles collectively contribute to dorsiflexion/plantarflexion, inversion/eversion, and longitudinal arch stabilization, enabling the assessment of adaptive neuromuscular strategies during landing from both kinetic and stability perspectives. Following established electrode placement guidelines [26], surface EMG sensors were placed on the TA, PL, MG, and LG muscles. Because surface EMG is not suitable for deep or small muscles, the activation patterns of the remaining muscles were estimated using OpenSim musculoskeletal simulations. Specifically, experimental kinematic and kinetic data were input into OpenSim to perform inverse dynamics and static optimization, allowing the estimation of muscle activations that could not be directly measured.

Prior to data collection, the skin over the lower-limb electrode sites was prepared by shaving excess hair and cleaning with alcohol to reduce skin impedance and improve signal quality [26]. Participants wore tight-fitting shorts and short-sleeved shirts and were familiarized with the experimental protocol. A static calibration trial was first recorded with participants standing in a standard anatomical posture to define segment coordinate systems and scale the musculoskeletal model. For the dynamic trials, participants performed a single-leg landing task from a platform elevated 30 cm above the ground using their dominant leg (defined as the leg used to kick a ball). Participants were instructed to land naturally and maintain single-leg support for approximately 3 s until postural stability was achieved. Trials meeting these criteria were considered successful and

Figure 1

Overview of the experimental procedure, data processing, and finite element modeling workflow: (a) schematic diagram of the experimental movement; (b) experimental setup and EMG acquisition; (c) verification of the accuracy of muscle activation in OpenSim; (d) extraction of muscle synergies using non-negative matrix factorization (NNMF); (e) *K*-means clustering results; (f) classification results based on Pearson correlation coefficients; (g) decomposed activation coefficients and synergy vectors; (h) CT/MRI scanning and data acquisition; (i) image processing and 3D reconstruction of the foot in Mimics; (j) surface refinement, segmentation, and mesh optimization in Geomagic Studio; (k) assembly, material assignment, and equivalent stress analysis in ANSYS Workbench; (l) validation of the finite element model through vertical displacement of the navicular bone

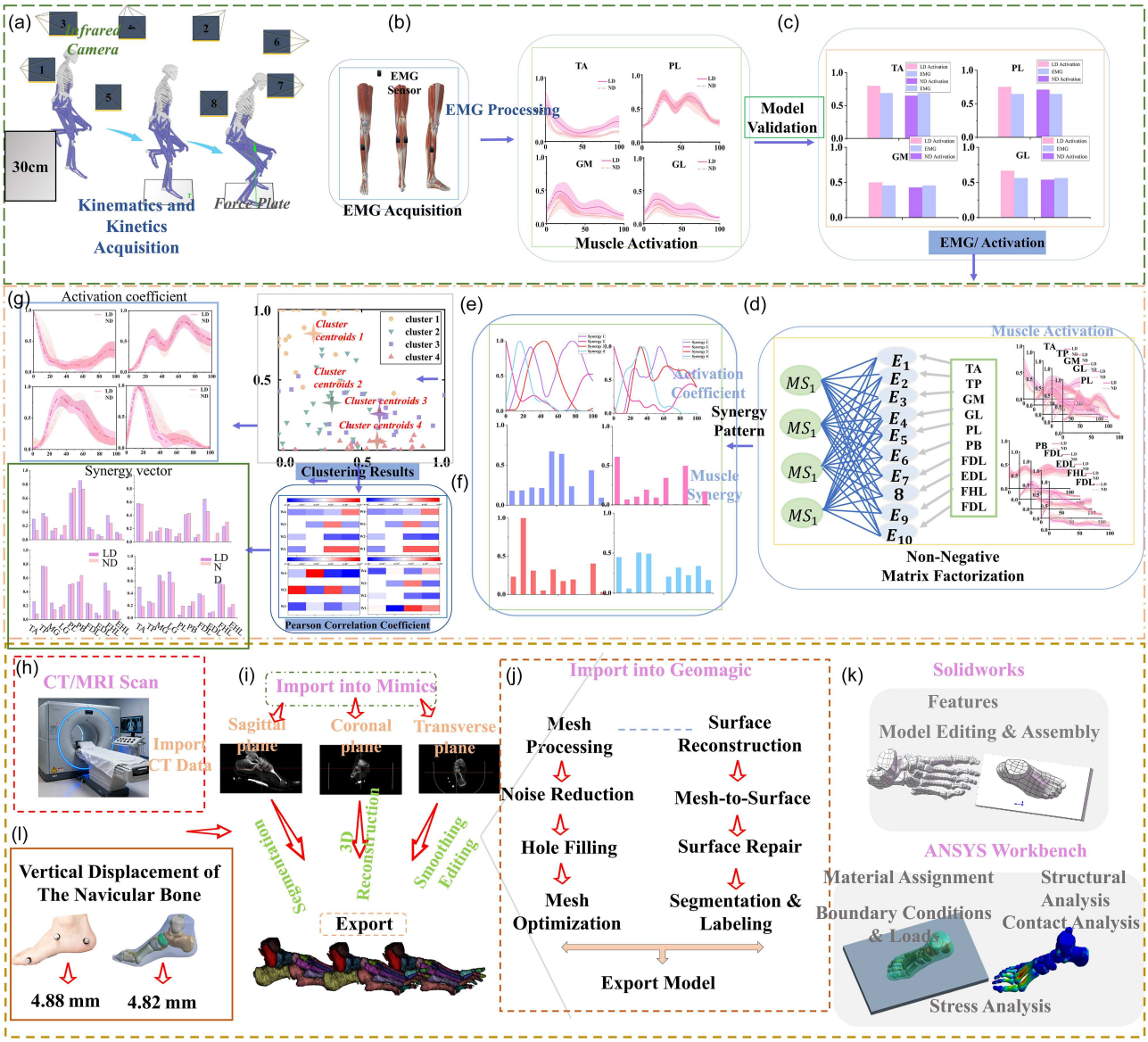

included in subsequent analyses. The experimental task is illustrated in Figure 1(a).

2.3. Kinematic, kinetic, and EMG data processing

The Vicon Nexus software was employed to export the motion capture data in C3D format for obtaining subjects' kinematic and kinetic information [27]. Subsequently, the data were further processed in MATLAB R2022a (The MathWorks, Natick, MA, USA), following a workflow that included coordinate system transformation, signal filtering, key data extraction, and data format conversion. Specifically, the coordinate systems of the kinematic and kinetic datasets were first transformed and aligned with the global coordinate system used in the subsequent OpenSim simulations, ensuring spatial consistency between the experimental data and the musculoskeletal models. To reduce the influence of noise on biomechanical computations, kinematic-related data and GRF data were filtered using a fourth-order zero-lag Butterworth low-pass filter, with cutoff frequencies set at 10 Hz and 20 Hz, respectively. After filtering, the kinematic data were converted into TRC (marker trajectories) file format, and the GRF data were converted into force platform data format, to meet the input requirements of OpenSim [25]. Biomechanical parameters were computed using OpenSim (Stanford University, Stanford, CA, USA). First, static calibration trials were imported into OpenSim 4.4, and a generic musculoskeletal model was

scaled using the Scale Tool to generate individualized models, ensuring that segment dimensions and muscle attachment locations were consistent with each participant's lower-limb anatomy. Subsequently, joint angles during the support phase were calculated using the inverse kinematics tool, and corresponding motion files were generated. To further improve the accuracy of dynamic calculations and reduce inconsistencies between model-driven forces and experimental measurements, the Residual Reduction Algorithm was applied to refine the kinematic data, thereby ensuring improved dynamic consistency [28].

For EMG signal processing, prior to full-wave rectification, the raw EMG signals were processed using a fourth-order band-pass filter (10–500 Hz) to remove low-frequency drift and high-frequency noise, thereby improving signal quality. The filtered signals were then smoothed using a 10 Hz low-pass filter to further reduce high-frequency artifacts. After preprocessing, the EMG activation signals of each muscle were normalized to the maximum activation observed across all trials, enhancing inter-subject comparability. To account for differences in trial duration, all signals were subsequently time-normalized to 101 data points, enabling consistent temporal alignment across participants [29].

Figure 1(b) illustrates the EMG activation profiles of 10 major lower-limb muscles in the LD and ND groups during the landing phase. To verify the reliability of muscle activation results derived from the OpenSim musculoskeletal model, experimentally measured EMG activation variables were compared with the muscle activations simulated by OpenSim. As shown in Figure 1(c), the simulated muscle activation patterns exhibited a high level of agreement with the experimental EMG signals in both temporal characteristics and overall trends, thereby validating the reliability of the simulation results.

2.4. Extraction of muscle synergy patterns based on the NNMF algorithm

As shown in Figure 1(d), to further investigate the neuromuscular coordination mechanisms involved in lower-limb control, muscle synergies were extracted from the processed EMG signals using non-negative matrix factorization (NNMF) [30, 31]. As EMG signals are inherently non-negative from a physiological perspective, NNMF provides a meaningful framework for decomposing multi-channel EMG data into a limited number of synergy modules without introducing sign reversals. This approach enables dimensionality reduction while preserving physiological interpretability. Prior to synergy analysis, the activation signals of each muscle channel were standardized to minimize potential bias arising from differences in signal amplitude across muscles. Specifically, the EMG activation of each channel was divided by its standard deviation to achieve unit variance normalization, as expressed in Equation (1):

$$\widehat{E}_{ij} = \frac{E_{ij}}{\sigma_j} \tag{1}$$

where E_{ij} represents the activation of the i-th muscle at the j-th sampling point, σ_j denotes the standard deviation of the j-th muscle, and $\widehat{E}_{ij}$ is the normalized activation value.

After normalization, the EMG data matrix E was organized into an $m \times n \times k$ structure, and the EMG matrix from each trial was independently input into the NNMF algorithm. NNMF decomposes the data into the product of two non-negative matrices: the synergy weight matrix W and the activation coefficient matrix H, as defined in Equation (2) [32, 33]:

$$E(m \times n) = W(m \times k) \times H(k \times n) + \varepsilon(m \times n) \tag{2}$$

where m denotes the number of recorded muscles and n denotes the number of time samples. The matrix Wrepresents the relative contribution (weighting) of each muscle within the identified synergy modules, while the matrix H describes the temporal activation profiles of these modules, reflecting the time-dependent neural modulation of muscle synergies. The residual matrix εcontains the portion of the signal not explained by the model. To ensure computational stability and reproducibility, fixed iteration limits and convergence criteria were applied during NNMF execution [30]. When multiple trials were available, the extracted synergy patterns were averaged or clustered across repetitions to obtain representative synergy modules, thereby improving the consistency and reliability of the analysis.

A small reconstruction error, ε, was allowed during NNMF decomposition, defined as [14]:

$$\varepsilon = E - WH \tag{3}$$

To determine the optimal number of muscle synergies, the number of synergy modules was increased iteratively, and the reconstruction quality was evaluated using the variance accounted for (VAF) criterion. The number of synergies was considered sufficient when both the global and individual muscle VAF satisfied the following conditions:

$$VAF_{Total} = 1 - \frac{\sum_{i=1}^{p}\sum_{j=1}^{n}(E_{ij} - \widehat{E}_{ij})^2}{\sum_{i=1}^{p}\sum_{j=1}^{n}E_{ij}^2} \geq 90\% \tag{4}$$

$$VAF_{Each_m} \geq 75\% \tag{5}$$

where p denotes the number of muscles and n denotes the number of time points [31]. These threshold criteria ensure that the extracted synergy patterns capture the majority of variance in the original EMG signals while preserving the physiological characteristics of neuromuscular coordination across different phases of movement.

2.5. Application of the *K*-means clustering algorithm in muscle synergy pattern classification

In this study, an unsupervised K-means clustering approach was applied to classify and identify muscle synergy patterns extracted from the EMG data. The purpose of clustering was to group synergy modules with similar structural characteristics, thereby revealing common neuromuscular coordination strategies across trials and participants. Because the performance of K-means clustering is highly dependent on the choice of cluster number, the optimal number of clusters was first determined using quantitative evaluation criteria (described below) to ensure an appropriate balance between within-cluster compactness and between-cluster separation. K-means clustering was selected due to its computational efficiency, simplicity, and suitability for high-dimensional datasets, making it particularly appropriate for large sets of muscle synergy features. Once the number of clusters was defined, the K-means algorithm initialized the cluster centroids randomly. During each iteration, data points were reassigned to the nearest centroid based on Euclidean distance, after which

the centroids were recalculated as the mean of all data points within each cluster. The iterative update of cluster centroids followed the convergence criterion defined as Raj and Palaniappan mentioned [34]:

$$\Delta C_k = \| C_k^{new} - C_k^{old} \| \quad (6)$$

where C_k^{new} represents the updated centroid of the kth cluster and C_k^{old} represents the centroid from the previous iteration. The clustering process was terminated when the displacement of all centroids fell below a predefined threshold, indicating convergence, or when the maximum number of iterations was reached [35]. To quantitatively assess clustering quality, the silhouette coefficient was calculated for each clustering solution. This metric evaluates the degree of similarity between data points within the same cluster relative to those in other clusters, providing an objective measure of clustering performance. Based on the silhouette analysis, the final clustering configuration was selected for subsequent analyses. The resulting clustering outcomes are illustrated in Figure 1(e).

2.6. Construction of the finite element model

During the experiment, the participant performed a step-down landing task from a platform with a height of 30 cm to obtain dynamic biomechanical data. Initial foot contact was defined as the instant when the vertical GRF exceeded 10 N, which served as a standardized criterion for identifying the onset of landing. Each participant completed 10 valid trials, and the averaged values across trials were used in subsequent analyses to reduce trial-to-trial variability and enhance data reliability. To develop a subject-specific FE model of the foot, the participant's right foot was scanned using computed tomography (CT) and magnetic resonance imaging (MRI). The imaging parameters were set as follows: tube voltage of 120 kV, tube current of 125 mA, slice thickness of 2 mm, and no interslice gap (Figure 1(h)). The combination of CT and MRI imaging enabled accurate reconstruction of both osseous structures and soft tissues, thereby improving anatomical fidelity. The acquired two-dimensional medical images were imported into Mimics 21.0 (Materialise, Leuven, Belgium) for tissue segmentation (Figure 1(i)), where individual bones and soft tissues were identified and extracted. The reconstructed surfaces were then imported into Geomagic Studio 2021 (Research Triangle Park, NC, USA) for geometric refinement, including smoothing, hole filling, and surface optimization, to ensure high-quality model geometry suitable for FE meshing (Figure 1(j)). Subsequently, all anatomical components were assembled in SolidWorks 2017 (Waltham, MA, USA) to generate a complete three-dimensional solid foot model [36]. Cartilage layers between adjacent bones were explicitly modeled as solid elements to allow for realistic articulation and load transmission across joints (Figure 1(k)). The final model was discretized using a tetrahedral mesh, which is well suited for representing complex bone and joint geometries while maintaining computational stability and automated mesh generation.

In the FE analysis, all biological tissues were assumed to be homogeneous, isotropic, and linearly elastic, and the corresponding material properties were assigned based on previously published Studies by Jitprapaikulsarn et al. [37] and Liu et al. [38] (Table 1). Dynamic kinematic and kinetic data, including GRF, collected during the landing task, were used to characterize movement mechanics. To ensure representative loading conditions, boundary conditions and external loads were defined using the averaged results from the 10 valid trials. The peak vertical GRF, measured as 900.55 N, was applied to the FE model as the primary loading input to simulate the mechanical environment experienced by the foot during landing.

Table 1
Material properties of the components in the finite element model

Model component	Elastic modules (MPa)	Poisson's ratio v	Topology structure
Bone	7300	0.3	3D-Tetrahedra
Cartilage	1	0.4	3D-Tetrahedra
Plate	17000	0.4	3D-Tetrahedra
Soft tissue	1.15	0.49	3D-Tetrahedra

2.7. Boundary and loading conditions

FE simulations of landing mechanics for both LD and ND were performed using the LS-DYNA explicit solver implemented in ANSYS Workbench 2021 (ANSYS Inc., Canonsburg, PA, USA). The explicit solver was selected because it is well suited for handling highly dynamic events, such as landing impacts, where large contact forces and rapid load transfer occur. A tetrahedral mesh was automatically generated for all anatomical components to accommodate the complex geometry of the foot while maintaining numerical stability and computational efficiency [36]. Contact interactions between adjacent model components were automatically detected using a surface proximity–based algorithm, allowing the identification of potential contact pairs without manual specification. The bone–cartilage interfaces were modeled using direct surface-to-surface contact, assuming frictionless interaction, as relative sliding between cartilage layers was considered minimal during the short landing phase. The surrounding soft tissue was represented as a deformable encapsulating layer, providing mechanical support and constraint to the skeletal structures. To replicate realistic foot–ground interaction during landing, a Coulomb friction coefficient of 0.2 was assigned to the foot–ground contact interface based on previous experimental and numerical studies by Athanasiou et al. [39]. The ground was modeled as a rigid surface and was fully constrained in all translational and rotational degrees of freedom. The foot model was positioned according to the experimentally measured landing posture. The ankle joint orientation was defined by the inclination angle between the tibial longitudinal axis and the foot longitudinal axis in the sagittal plane. The global coordinate system of the FE model was aligned with that used in OpenSim, ensuring consistency between experimental kinematic data and numerical simulations. Dynamic boundary conditions and external loads were derived from experimental measurements. Specifically, the averaged displacement data and GRF obtained from valid trials were applied to the model as loading inputs, thereby representing typical landing conditions while minimizing trial-to-trial variability. To evaluate internal stress responses within the metatarsal and phalangeal bones during landing, the von Mises equivalent stress was calculated as the primary outcome variable. This stress measure reflects the combined effect of multiaxial loading according to distortion energy theory and is widely used to assess overall stress states in biological tissues. The Von Mises stress was computed as Gefen mentioned [40]:

$$\sigma_v = \sqrt{\frac{(\sigma_1 - \sigma_2)^2 + (\sigma_2 - \sigma_3)^2 + (\sigma_3 - \sigma_1)^2}{2}} \quad (7)$$

where σ_1, σ_2, and σ_3 represent the three principal stresses at each node. This metric enables quantitative comparison of stress magnitudes across different anatomical regions. Except for the encapsulating soft tissue and skin, all materials were assumed to be homogeneous, isotropic, and linearly elastic, with material properties assigned based on previously published literature by Zhou et al. [36] and Jitprapaikulsarn et al. [37]. To avoid issues associated with the selection of a reference condition, symmetric percentage differences were used to quantify relative differences in peak von Mises stress.

2.8. Validation of the finite element model

To assess the reliability of the constructed FE foot model, a validation analysis was performed by simulating a normal weight-bearing landing condition and comparing the predicted deformation with corresponding experimental measurements reported in the literature by Liu et al. [38]. Model validation is a critical step to ensure that the numerical model can realistically reproduce foot deformation under physiological loading conditions before being used for further stress analysis. In the validation simulation, full body weight was applied to the plantar surface of the foot model as an external load to replicate a static weight-bearing condition. In addition, representative muscle forces generated by the medial gastrocnemius, lateral gastrocnemius, and tibialis anterior were incorporated into the model to better approximate physiological loading during stance [40, 41]. These muscle forces were applied along anatomically defined muscle lines of action, thereby reproducing the stabilizing role of lower-leg musculature on the foot arch. The vertical displacement of the navicular bone was selected as the primary validation parameter, as navicular motion is widely recognized as a clinically and biomechanically relevant indicator of overall foot deformation and arch behavior under load. In the experimental reference data, a measurement point was defined at the medial tuberosity of the navicular bone, and its vertical displacement was recorded under full weight-bearing conditions [38]. An identical anatomical landmark was identified in the FE model to ensure consistency between experimental and numerical measurements. The FE simulation predicted a maximum vertical displacement of 4.88 mm at the navicular bone. This result closely matched the experimentally measured displacement of 4.82 mm, yielding a relative difference of less than 1.3%. The strong agreement between simulated and experimental values indicates that the FE model can accurately capture the deformation behavior of the foot under loading conditions. Therefore, the validated model was deemed suitable for subsequent stress and strain analyses. The validation results are illustrated in Figure 1(l).

2.9. Statistical analysis

Prior to statistical analysis, the normality of the dataset was evaluated using the Shapiro–Wilk test to ensure the suitability of parametric testing. Independent samples *t*-tests were then applied to examine group differences in plantar parameters during the landing phase. All data were processed through custom MATLAB scripts developed for statistical parametric mapping (SPM) analysis and were time-interpolated to 101 equally spaced points to enable point-by-point statistical comparisons [33]. Statistical analyses were carried out using the open-source SPM1d package, and the level of significance was set at $p < 0.05$ [42, 43].

To further assess the similarity of the extracted muscle synergies, Pearson correlation analysis was performed (as shown in Figure 1(f)). This method was selected because it quantifies the degree of linear association between two continuous variables, allowing a direct comparison of activation patterns across synergy vectors (Figure 1(g) shows the results classified based on Pearson correlation coefficients). In this context, higher correlation values indicate more similar muscle activation profiles. A correlation coefficient (r) approaching 1 reflects a strong similarity, values around 0 suggest independence, while negative values indicate an inverse activation tendency [44].

$$r = \frac{\sum(x_i - \overline{x})(y_i - \overline{y})}{\sqrt{\sum(x_i - \overline{x})^2 \sum(y_i - \overline{y})^2}} \tag{8}$$

Here, r denotes the Pearson correlation coefficient, x_i and y_i are the observed values of the two variables, and x and y represent their means. Correlation strength was interpreted as follows: 0.7–1.0 (strong), 0.3–0.7 (moderate), and below 0.3 (weak). In this study, synergy pairs with $r > 0.6$ were considered highly similar and grouped together for classification.

3. Results

3.1. Kinematic and kinetic results in the sagittal plane

Figure 2(a) illustrates the SPM analysis for the ankle joint results, indicating that the LD group exhibited a notably higher dorsiflexion angle compared to the ND group throughout the 0–96.01% stance phase ($p < 0.001$). Moreover, the LD group demonstrated a significantly greater moment than the ND group at 11.52–33.32% ($p = 0.001$) and 52.07–100% ($p < 0.001$) of the stance phases. The LD group demonstrated a significantly smaller velocity than the ND group at 0–5.64% ($p = 0.031$) of the stance phases.

SPM analysis for the metatarsophalangeal joint (MTP) showed that the LD group exhibited a significantly greater plantarflexion angle than the ND group throughout the 0–5.43% stance phase ($p < 0.001$) and a notably higher moment than the ND group during the 2.44–72.26% stance phases ($p < 0.001$). The LD group demonstrated a significantly greater velocity than the ND group at 0–9.87% ($p = 0.007$) of the stance phases (Figure 2b).

Meanwhile, significant differences were observed between the LD group and the ND group in peak ankle joint parameters. Specifically, the maximum angle ($p < 0.001$), minimum angle ($p < 0.001$), and range of motion ($p < 0.001$) differed significantly; for joint moments, the minimum moment ($p < 0.001$) and range of motion ($p < 0.001$) were significantly different, while the maximum moment showed no significant difference ($p = 0.683$); for angular velocity, the maximum ($p = 0.028$), minimum ($p < 0.001$), and range of motion ($p < 0.001$) all exhibited significant differences (Figure 2c).

Significant differences were also observed between the LD group and the ND group in peak MTP joint parameters. Specifically, the maximum angle ($p = 0.014$, $d = 2.56$), minimum angle ($p < 0.001$, $d = 3.13$), and range of motion ($p < 0.001$, $d = 2.38$) differed significantly; for joint moments, the maximum moment ($p = 0.032$, $d = 1.26$), minimum moment ($p < 0.001$, $d = 4.70$), and range of motion ($p < 0.001$, $d = 3.12$) were significantly different; for angular velocity, the minimum ($p < 0.001$, $d = 2.89$) and range of motion ($p < 0.001$, $d = 2.86$) showed significant differences, whereas the maximum angular velocity did not differ significantly ($p = 0.751$, $d = 0.14$) (Figure 2d).

Figure 2

Comparison of lower-limb kinematics and kinetics between Latin dancers (LD) and non-dancers (ND): (a) ankle joint kinematic and kinetic profiles with statistical parametric mapping (SPM) analysis; (b) MTP joint kinematic and kinetic profiles with SPM analysis; (c) comparison of ankle joint peak parameters; (d) comparison of MTP joint peak parameters

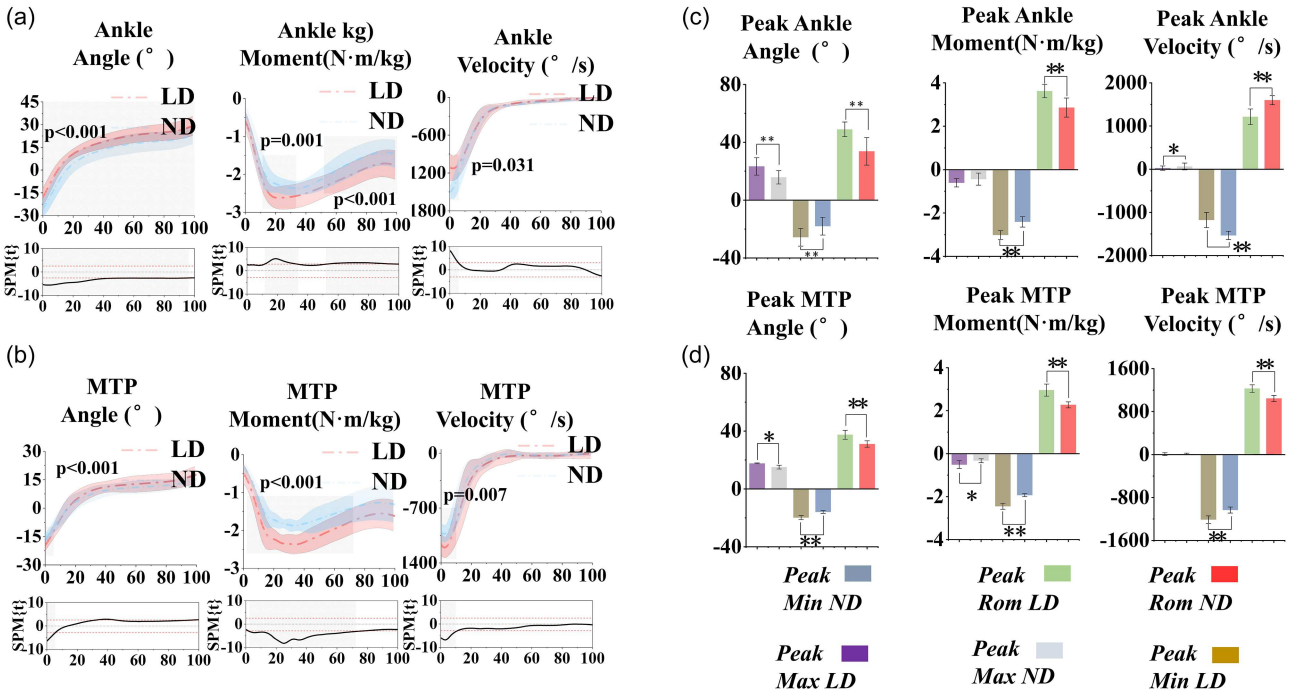

Figure 3

Verification of muscle activation accuracy and identification of muscle synergies: (a) comparison between experimentally recorded EMG signals and OpenSim-simulated activations; (b) preprocessed EMG signals used as inputs for NNMF decomposition; (c) determination of the optimal number of muscle synergies based on variance accounted for (VAF); (d) confirmation of the final synergy number through clustering validation

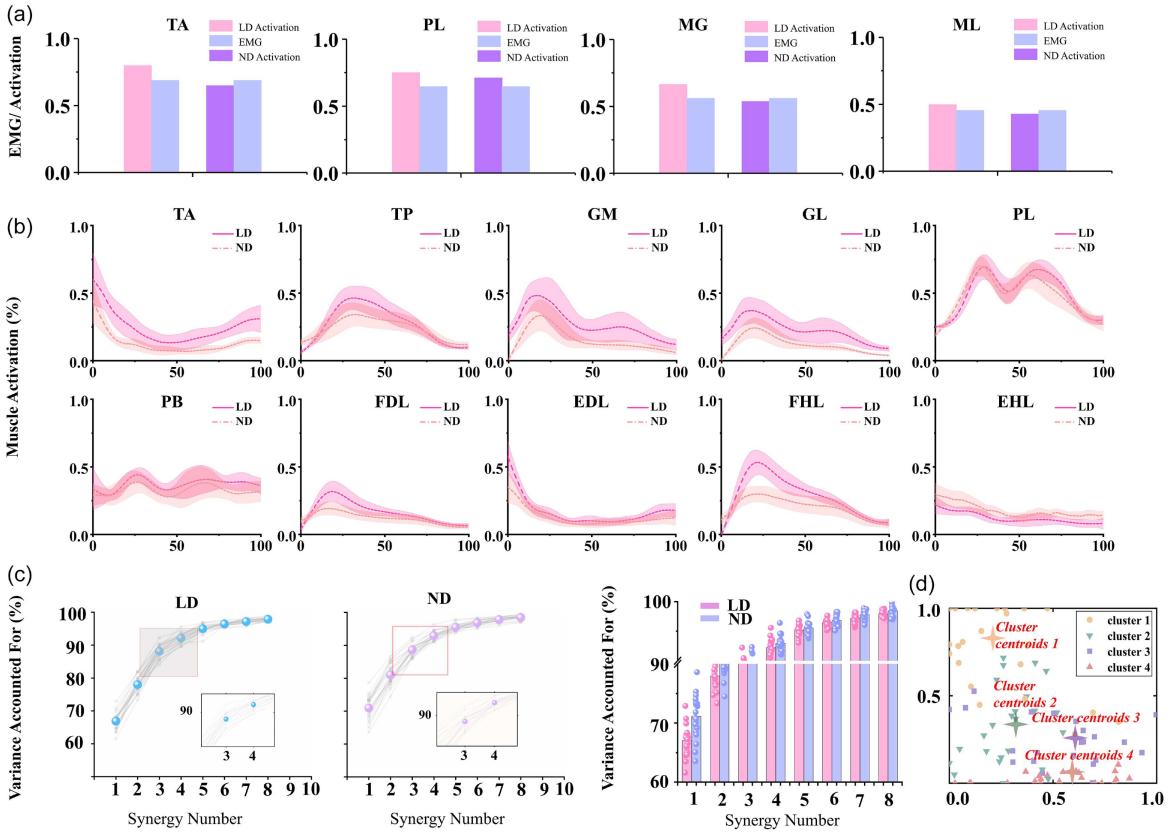

3.2. Selection of the number of synergies

As illustrated in Figure 3(a), the study first compared EMG signals directly recorded from the medial gastrocnemius, lateral gastrocnemius, tibialis anterior, and peroneus longus with the simulated EMG signals obtained from OpenSim. The results demonstrated that the OpenSim-derived signals accurately reflected the actual muscle activation patterns. Based on this validation, the activation levels of 10 major muscles surrounding the ankle and MTP joints were calculated for dancers and non-dancers during the landing phase (Figure 3b). The processed EMG data were then input into an NNMF algorithm to extract the activation coefficients and muscle synergy matrices (Figures 4 and 5).

To systematically assess the similarity and number of distinct synergies, *K*-means clustering analysis was further applied to the extracted NNMF modes. The results indicated no significant difference in the number of synergies between the LD group and the ND group during the landing task (Figure 3(c). In most cases, using four muscle synergies, both the LD and ND groups achieved a global variance accounted for (global VAF) exceeding 90%, with local muscle VAFs for each individual muscle exceeding 75% (Table 2). No statistically significant differences were observed between the LD and ND groups in terms of the number of muscle synergies, global VAF, or local muscle VAF. Further analysis identified 3–5 synergies, with four synergies being sufficient to adequately reconstruct the original EMG signals and achieve the optimal clustering performance. Accordingly, four fundamental synergies were established (Figure 3d), which were subsequently used for the analysis of muscle coordination and neuromuscular control strategies.

Notably, the number of muscle synergies identified in the present study is consistent with previous findings on lower-limb neuromuscular coordination during dynamic tasks such as walking, running, and landing. Existing studies generally indicate that, during dynamic lower-limb movements, 3–5 muscle synergies are sufficient to explain most of the variance in EMG signals when using NNMF. In the present study, four muscle synergies achieved a high level of VAF, suggesting that this number of synergies effectively captures the primary coordination patterns of lower-limb muscles during the landing task.

3.3. Similarity of muscle synergies

Based on the silhouette coefficient to assess clustering quality, the centroids of the four clusters were used as reference synergies, and Pearson correlation coefficients were employed to classify the synergy patterns of each participant (Figure 6).

3.4. Functional interpretation of muscle synergies

A muscle was considered active when its weight exceeded 0.3, a threshold commonly used in muscle synergy analysis to identify muscles that contribute meaningfully to the synergy. Compared with the ND group, the LD group demonstrated earlier activation onsets and higher activation amplitudes in several synergies during the landing phase. Similar phase-dependent muscle synergy structures have been reported in state-of-the-art studies

Figure 4

The extracted synergy vectors matrix and activation coefficient matrix from six subjects in the Latin dancers (LD) group are presented, with activation coefficient results displayed in rows 1 and 6 and the remaining rows depicting the synergy vectors

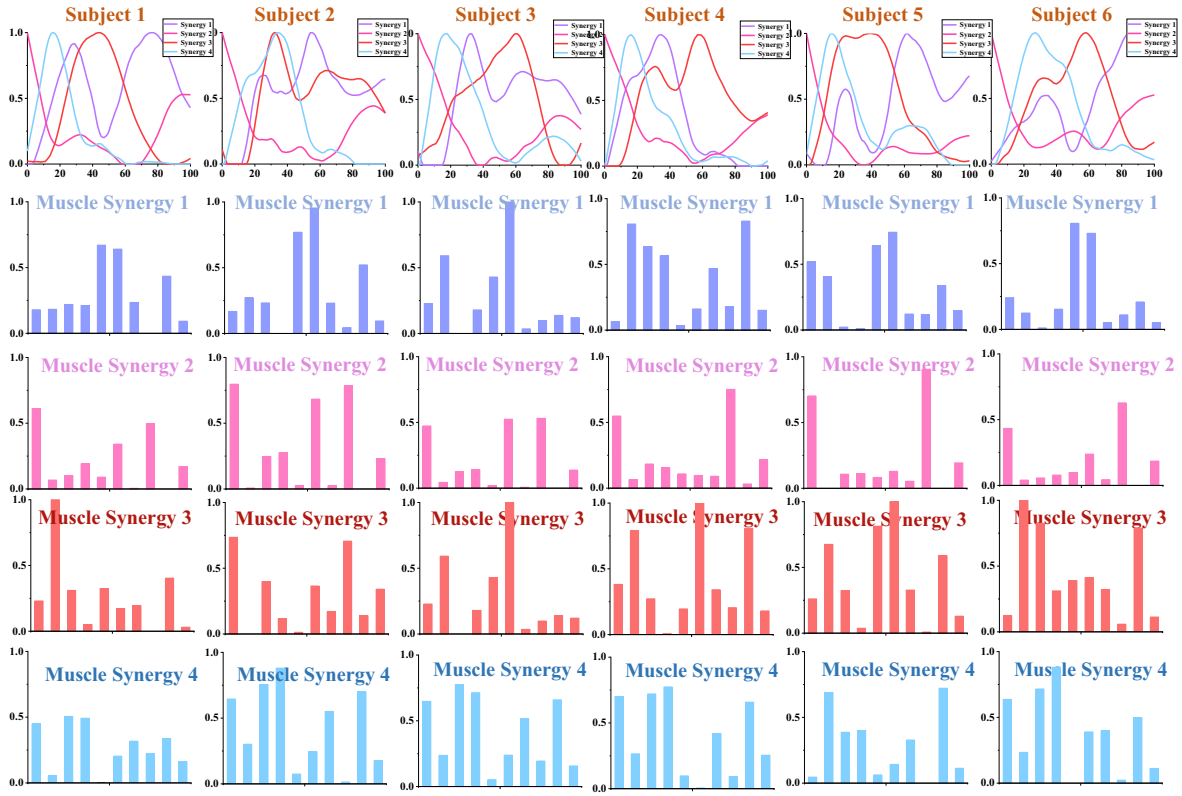

Figure 5
The extracted synergy vectors matrix and activation coefficient matrix from six subjects in the non-dancers (ND) group are presented, with activation coefficient results displayed in rows 1 and 6 and the remaining rows depicting the synergy vectors

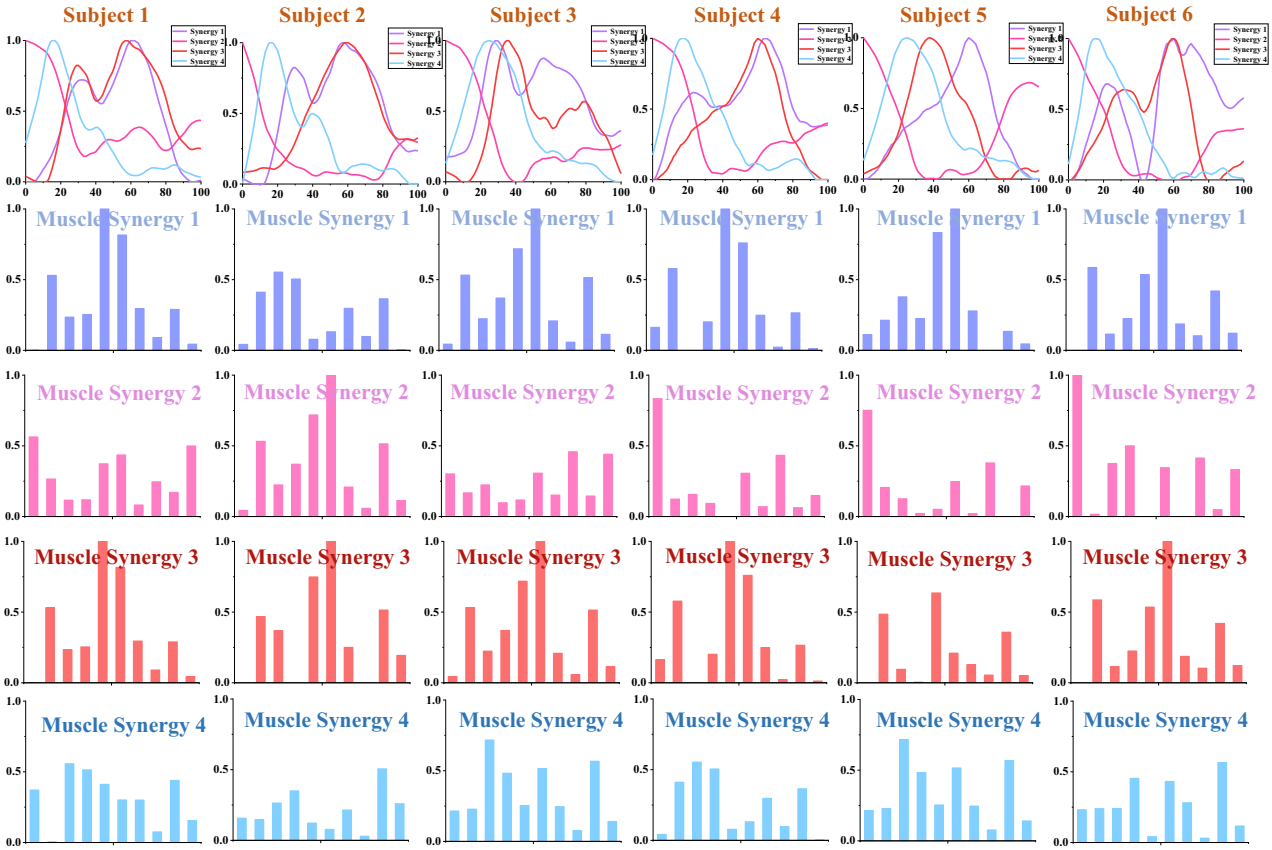

Table 2
Descriptive data on the number of muscle synergies, global VAF, and local VAFs for each group

	LD group Mean (SD)	ND group Mean (SD)	*p*-value
N_{syn}	3.95 (0.49)	3.79 (0.41)	0.223
Global VAF (%)			
With three synergies	88.11 (1.98)	88.96 (1.84)	0.128
With four synergies	92.16 (1.51)	93.07 (1.35)	0.031*
With five synergies	94.96 (1.32)	95.63 (0.98)	0.061
Local VAFs with four synergies (%)			
TA	93.95 (2.34)	92.74 (4.50)	0.281
TP	92.60 (3.67)	93.90 (3.70)	0.260
GM	91.22 (4.39)	90.69 (5.59)	0.737
GL	91.02 (2.53)	92.59 (3.24)	0.088
PL	90.63 (3.88)	92.46 (2.61)	0.080
PB	94.17 (2.78)	95.07 (2.46)	0.275
FDL	91.11 (3.69)	92.40 (2.37)	0.186
EDL	90.12 (4.90)	89.12 (5.73)	0.547
FHL	94.23 (1.62)	93.04 (3.41)	0.084
EHL	87.87 (3.86)	89.40 (4.92)	0.269

Figure 6
Correlation coefficients between synergy vectors and reference synergies for the subjects in the healthy group

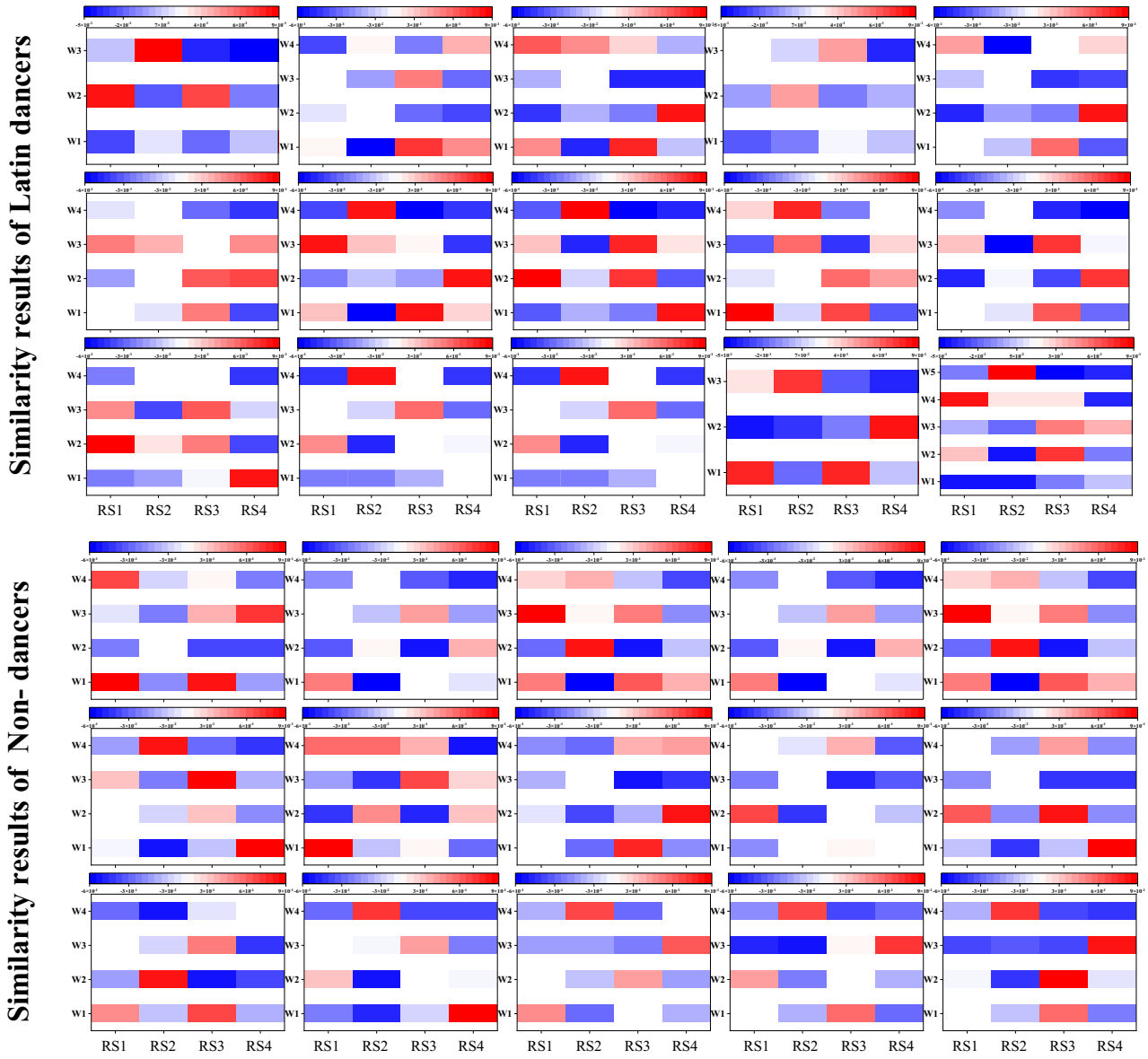

Note: W: synergy vectors, RS: reference synergy

investigating lower-limb neuromuscular coordination during dynamic tasks such as landing and running. The functional characteristics of each synergy observed in the present study are described below (Figure 7).

Synergy 1 contact to early absorption (deceleration phase): The activation coefficient curve in the LD group peaked earlier, around 5–10% of stance, than in the ND group. This indicates a more anticipatory activation of the dorsiflexors to reduce impact forces. The LD group also showed slightly higher peak amplitudes, reflecting stronger involvement of the tibialis anterior and extensor digitorum longus during initial contact. The ND group showed larger inter-individual variability during the early stance phase, reflected by wider standard deviation bands, while the LD group demonstrated more consistent activation patterns.

Synergy 2 lateral arch stabilization: The LD group exhibited an earlier and more compact activation peak (approximately 30–40% of stance), whereas the ND group showed a broader and delayed activation profile. Similar lateral stabilization synergies dominated by the peroneus longus have been widely reported in previous advanced studies on foot arch control during dynamic weight-bearing tasks. The greater weighting of the peroneus longus and flexor digitorum longus in the LD group suggests improved lateral arch regulation, consistent with state-of-the-art observations in trained populations.

Synergy 3 forefoot support and medial stability: The LD group reached peak activation slightly earlier, with higher amplitudes in the flexor hallucis longus, indicating more efficient load transfer and enhanced forefoot stability. Comparable forefoot-dominant synergies have been identified in prior studies examining mid-stance control during dynamic lower-limb movements. In contrast, the delayed and weaker activation observed in the ND group suggests less effective medio-lateral stabilization,

Figure 7

Muscle synergies during landing from a 30-cm platform in Latin dancers (LD) and non-dancers (ND), analyzed from initial contact to peak knee flexion. Upper panels show the activation coefficients (C); lower panels show the synergy vectors (W). Four modules were identified by NMF: (a) Synergy 1, contact to early absorption; (b) Synergy 2, lateral arch stabilization; (c) Synergy 3, forefoot support and medial stability; (d) Synergy 4, late-stance energy dissipation and propulsion

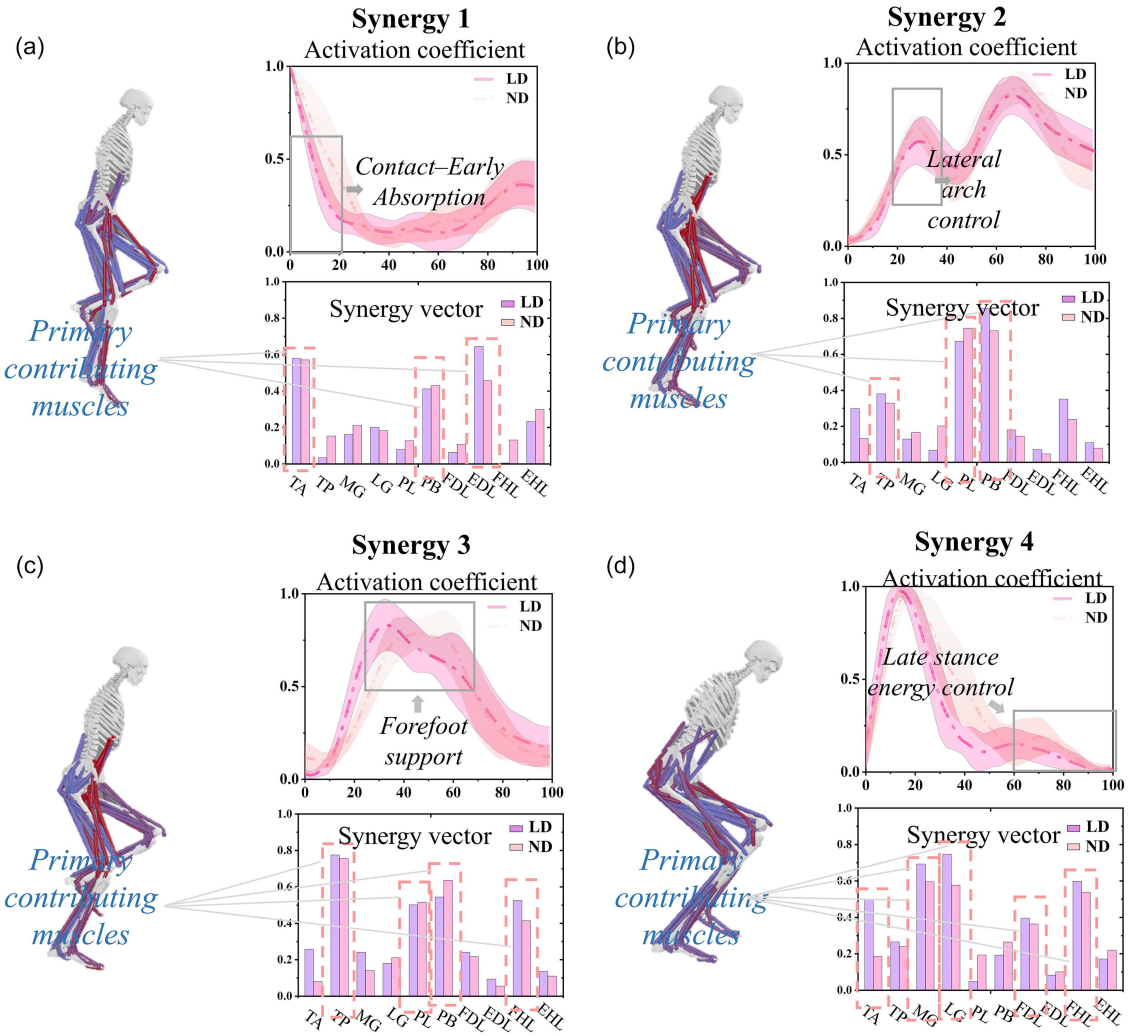

aligning with patterns previously reported in untrained individuals. Notably, greater inter-individual variability was observed in the LD group during the forefoot support phase, as indicated by the wider standard deviation bands, whereas the ND group showed more clustered activation patterns in this phase.

Synergy 4 late-stance energy dissipation and propulsion: During late stance, the LD group demonstrated a shorter but sharper activation burst of the gastrocnemius and flexor hallucis longus, whereas the ND group showed delayed and prolonged activation. This timing-sensitive plantarflexor synergy closely resembles those described in state-of-the-art studies on propulsion and energy dissipation during landing and push-off phases. The observed pattern indicates that dancers rely on more precise temporal modulation of plantarflexor activity to maintain postural stability and control energy dissipation.

3.5. Finite element analysis

Figure 8 illustrates the von Mises stress distribution of the metatarsals and proximal phalanges in the LD group and the ND group during a 30-cm drop landing. Both groups exhibited evident stress concentrations in the first and second metatarsals, while the third to fifth metatarsals showed relatively lower stress levels. Compared with the ND, the dancer group demonstrated higher stress values in the first and second metatarsals and their corresponding phalanges, with high-stress regions mainly located on the dorsal and plantar surfaces of the metatarsals. In contrast, the ND group showed a more uniform stress distribution with generally lower magnitudes, indicating a more dispersed load across the forefoot. Overall, these results suggest that LD experience more pronounced forefoot and medial stress concentration during landing. As shown in Figure 8, the peak von Mises stresses of the first to fifth metatarsals in the dancer group were 17.12, 17.86, 11.48, 7.64, and 5.21 MPa, respectively; the corresponding peak von Mises stresses of the first to fifth proximal phalanges were 16.09, 11.38, 7.43, 4.68, and 2.85 MPa. In the non-dancer group, the peak von Mises stresses of the first to fifth metatarsals were 15.55, 17.33, 11.56, 7.83, and 5.09 MPa, respectively; the corresponding peak von Mises stresses of the first to fifth proximal phalanges were 15.43, 11.36, 7.16, 4.70, and 2.77 MPa.

Figure 8
Von Mises stress distribution of metatarsals and proximal phalanges in Latin dancers (LD) and non-dancers (ND) during a 30-cm drop landing

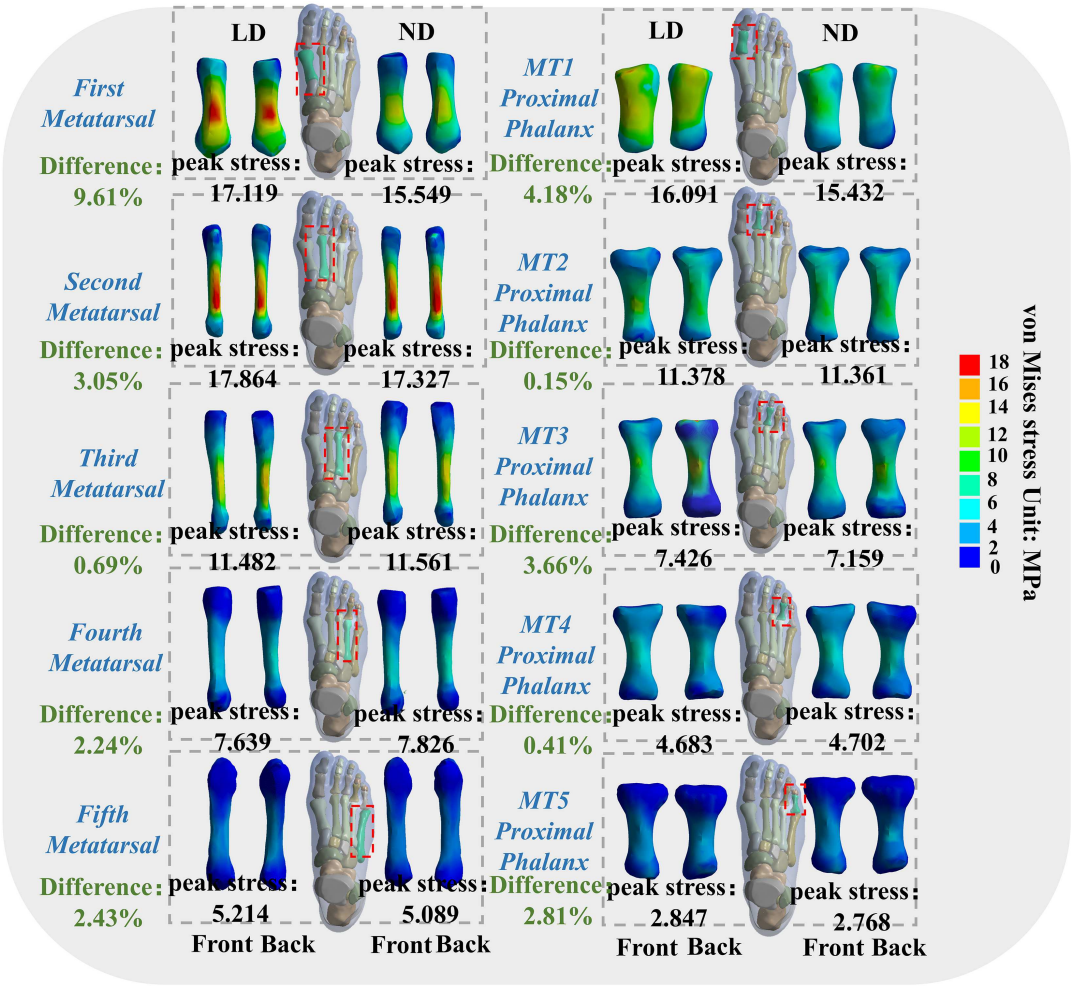

4. Discussion

This study integrated kinematic–kinetic analysis, electromyographic synergy modeling, and FE simulation to elucidate the adaptive effects of dance training on the neuro-biomechanical system of the lower limbs from multiple perspectives. The results demonstrated that long-term dance training induces a multilevel synergistic remodeling centered on optimized feedforward regulation, reflected in coupled adaptations across the functional, neural control, and structural domains.

At the functional level, dancers exhibited greater flexion angles and joint moments at the ankle and MTPs during landing tasks, indicating enhanced capacities for energy absorption and propulsion [45, 46]. Increased joint flexion allows for extended buffering time and dispersion of impact forces, while higher joint moments suggest a more efficient collaboration between the ankle–metatarsal complex in energy storage and release [45]. Such an efficient energy absorption–release conversion mechanism forms the foundation for stable landings and effective propulsion [47, 48]. Compared with unidirectional activities such as running or jumping, the multidirectional, rhythmic, and highly controlled nature of dance training promotes the development of more sophisticated energy regulation strategies and postural stabilization mechanisms [49]. The dancers' lower ankle angular velocity suggests an active dorsiflexion landing strategy that anticipates impact absorption [46]. This control feature reflects a training-induced energy management mechanism based on predictive regulation, laying the groundwork for earlier and more focused synergistic activation at the neural control level.

At the neural control level, although the number of synergies was comparable between dancers and non-dancers, the former displayed earlier peak activation, higher amplitude, and more compact temporal structures, indicating greater efficiency in the temporal organization of neuromuscular control [14]. The characteristic of early, high-amplitude synergy activation exemplifies the core mechanism of optimized feedforward regulation—pre-activation and postural preparation of the muscles before external impact, enabling rapid and stable responses. Furthermore, dancers developed a distal-dominant synergy pattern centered on the foot and ankle muscles. Although proximal muscles were not directly measured, the dancers' earlier and more concentrated activation with a higher distal contribution suggests a functional shift toward distal regulation, consistent with previous findings that skill learning enhances control precision and hierarchical optimization [49].

Specifically, during the initial contact phase, dancers showed earlier activation of the TA, which eccentrically controlled ankle dorsiflexion to attenuate impact transmission, demonstrating a

typical feedforward stabilization pattern. In the mid-phase, both groups utilized the TP, PL, and PB to stabilize the ankle joint, but dancers additionally recruited the FHL, forming a "multi-muscle synergistic activation mechanism." This mechanism indicates greater neural control capacity and muscle recruitment efficiency, enabling higher coordination in impact absorption and posture adjustment [50]. During the forefoot support phase, as the center of mass shifted fully to the forefoot, the dancers showed earlier and stronger activation of TP and FHL, suggesting precise preparation for support through distal control. Given that Latin dance involves frequent forefoot loading and rapid weight shifts, dancers appear to have developed a task-specific control pattern that allows agile postural adjustments upon landing. The prominent role of FHL further highlights its critical contribution to impact absorption and load distribution, indicating enhanced neural sensitivity in its control following dance training [51]. In the late landing phase, the main synergistic muscles in dancers demonstrated greater activation amplitudes and earlier activation timing than in ND, enabling quicker achievement of postural stability. Collectively, these features suggest that dance training enhances the predictive optimization and dynamic balance of the neuromuscular system through feedforward control mechanisms.

FE analysis showed that the two groups exhibited similar overall stress distribution patterns, with peak stresses primarily concentrated around the second MTP [52]. However, more pronounced stress concentrations were observed in the first and second metatarsals and their corresponding phalanges in dancers. These differences suggest that distinct landing mechanics may place greater mechanical demands on the forefoot, potentially facilitating more effective load transfer and support of the foot arch. This forefoot-dominant functional pattern may help reduce localized stress associated with excessive inversion or eversion, thereby improving impact attenuation. Similar forefoot loading patterns have been widely reported in studies of ballet dancers. Previous research has shown that dancers who are repeatedly exposed to sustained forefoot support and high demands at the MTPs are more susceptible to stress-related injuries and fatigue fractures of the first and second metatarsals. Epidemiological evidence further indicates that forefoot-related injuries account for approximately one-third to one-half of all foot and ankle injuries in dancers, with the first and second metatarsals being among the most commonly affected sites due to repetitive forefoot loading [53–55]. Nevertheless, while such reinforcement of forefoot loading may enhance support and energy transmission, it could also increase the risk of localized overload. Prolonged forefoot loading may contribute to metatarsal stress injuries and soft tissue fatigue, and repetitive flexion–extension at the MTPs may elevate shear stress at the first MTP, increasing the risk of cartilage degeneration [56, 57]. Therefore, future training and rehabilitation strategies should aim to improve foot function and stability while maintaining a balanced distribution of loads and adequate recovery, in order to reduce the risk of chronic injury.

In summary, dance training enhances foot–ankle coordination, optimizes load transmission pathways, and contributes to the stability of the medial arch, leading to adaptive changes in neural control and mechanical output. These findings highlight the high plasticity of the neuro-biomechanical system during complex skill acquisition and provide empirical evidence for understanding the hierarchical adaptive mechanisms induced by long-term training. Moreover, they offer valuable insights for the development of precision training programs, injury prevention strategies, and rehabilitation interventions. In addition, we acknowledge that this study has certain limitations. First, only female participants were included, which may limit the generalizability of the findings. Future studies should consider including male participants. The FE model was validated only under a static weight-bearing condition. Although this approach serves as a baseline plausibility check, it does not adequately capture the complex, time-dependent loading characteristics of dynamic dance landings. Future studies should incorporate dynamic experimental validation to improve the ecological validity of the model. Although applying group-specific parameters from different groups to a single FE model is a reasonable approach for isolating loading-related effects in the present study, it may limit the interpretation of the results by not accounting for potential differences in foot structure between groups.

5. Conclusion

Dance training, through long-term repetitive support and center-of-mass transfer movements, induces a feedforward-driven neuro-biomechanical coupling model. Within this model, synergistic reorganization of distal muscles and structural adaptations act in concert: the nervous system predicts impact and adjusts posture by pre-activating key muscle groups, while the musculoskeletal system reinforces this functional control through structural remodeling. The coupled remodeling of these systems markedly enhances impact absorption efficiency and postural stability. This finding highlights the high plasticity of the neuro-biomechanical system under complex skill training and provides a new theoretical framework and empirical foundation for precision training, injury prevention, and rehabilitation interventions.

Funding Support

This study was sponsored by the Zhejiang Provincial Natural Science Foundation of China for Distinguished Young Scholars (LR22A020002), Zhejiang Provincial Key Research and Development Program of China (2023C03197), Ningbo key R&D Program (2022Z196), National Key Research and Development Program of China (2024YFC3607305), Zhejiang Rehabilitation Medical Association Scientific Research Special Fund (ZKKY2023001), and China Scholarship Council.

Ethical Statement

This study was conducted in accordance with the principles of the Declaration of Helsinki and was approved by the Ethics Committee of Ningbo University (Approval No. TY202481). Prior to the experiments, all participants provided written informed consent.

Conflicts of Interest

The authors declare that they have no conflicts of interest to this work.

Data Availability Statement

The data that support the findings of this study are openly available in Figshare at https://doi.org/10.6084/m9.figshare.31333936.

Author Contribution Statement

Xiangli Gao: Conceptualization, Methodology, Software, Validation, Formal analysis, Investigation, Resources, Data curation, Writing – original draft, Writing – review & editing, Visualization. **Datao Xu:** Methodology, Resources. **Minjun Liang:** Methodology, Resources. **Zanni Zhang:** Investigation, Data curation. **Tianle Jie:** Investigation, Data curation. **Huiyu Zhou:** Methodology. **Jingyi Ye:** Methodology. **Zsolt Radak:** Supervision. **Yaodong Gu:** Supervision, Project administration, Funding acquisition.

References

[1] Fyfe, J. J., Hamilton, D. L., & Daly, R. M. (2022). Minimal-dose resistance training for improving muscle mass, strength, and function: A narrative review of current evidence and practical considerations. *Sports Medicine*, *52*(3), 463–479. https://doi.org/10.1007/s40279-021-01605-8

[2] Wen, J., Leng, L., Hu, M., Hou, X., & Huang, J. (2023). Effects of whole-body vibration training on cognitive function: A systematic review. *Frontiers in Human Neuroscience*, *17*, 854515. https://doi.org/10.3389/fnhum.2023.854515

[3] Welte, L., Holowka, N. B., Kelly, L. A., Arndt, A., & Rainbow, M. J. (2023). Mobility of the human foot's medial arch helps enable upright bipedal locomotion. *Frontiers in Bioengineering and Biotechnology*, *11*, 1155439. https://doi.org/10.3389/fbioe.2023.1155439

[4] Yildiz, R., Yildiz, A., Camli, O., Akkaya, H., Aydin, M., & Basaran, Z. (2025). Effect of plantar sensory stimulation on sensorimotor organization in general joint hypermobility: A randomized controlled study. *Healthcare*, *13*(20), 2572. https://doi.org/10.3390/healthcare13202572

[5] Wang, B., Shen, B., Xiao, S., Zhou, J., & Fu, W. (2024). Effects of four weeks intervention combining high-definition transcranial direct current stimulation and foot core exercise on dynamic postural stability. *Journal of Biomechanics*, *177*, 112418. https://doi.org/10.1016/j.jbiomech.2024.112418

[6] Che, L., Zhou, Y., & Wang, Y. (2025). Effects of 12-week pilates reformer training on the biomechanics of Latin dance Cha-Cha circle chasing technique. *Frontiers in Physiology*, *16*, 1549389. https://doi.org/10.3389/fphys.2025.1549389

[7] Gao, X., Xu, D., Baker, J. S., Ee-Chon, T., Liang, M., & Gu, Y. (2024). Exploring biomechanical variations in ankle joint injuries among Latin dancers with different stance patterns: Utilizing OpenSim musculoskeletal models. *Frontiers in Bioengineering and Biotechnology*, *12*, 1359337. https://doi.org/10.3389/fbioe.2024.1359337

[8] Liu, Y.-T., Lin, A.-C., Chen, S.-F., Shih, C.-J., Kuo, T.-Y., Wang, F.-C., . . . , & Lee, A. P. (2022). Superior gait performance and balance ability in Latin dancers. *Frontiers in Medicine*, *9*, 834497. https://doi.org/10.3389/fmed.2022.834497

[9] Stawicki, P., Wareńczak, A., & Lisiński, P. (2021). Does regular dancing improve static balance? *International Journal of Environmental Research and Public Health*, *18*(10), 5056. https://doi.org/10.3390/ijerph18105056

[10] Virtanen, N., Tiippana, K., Tervaniemi, M., Poikonen, H., Anttila, E., & Kaseva, K. (2022). Exploring body consciousness of dancers, athletes, and lightly physically active adults. *Scientific Reports*, *12*(1), 8353. https://doi.org/10.1038/s41598-022-11737-0

[11] Senger, D., Panosso, I., Likes Borba, B., Lucchese Gavioli, I., & Nogueira Haas, A. (2024). Effects of training protocols on dancers' balance: A systematic review. *Journal of Bodywork and Movement Therapies*, *40*, 366–372. https://doi.org/10.1016/j.jbmt.2024.04.013

[12] Bai, X., Hou, X., Lv, D., Wei, J., Song, Y., Tang, Z., . . . , & Liu, J. (2024). Development of an interpretable model for foot soft tissue stiffness based on gait plantar pressure analysis. *Frontiers in Bioengineering and Biotechnology*, *12*, 1482382. https://doi.org/10.3389/fbioe.2024.1482382

[13] Bruyneel, A.-V., Chavet, P., Bollini, G., & Mesure, S. (2010). Gait initiation reflects the adaptive biomechanical strategies of adolescents with idiopathic scoliosis. *Annals of Physical and Rehabilitation Medicine*, *53*(6-7), 372–386. https://doi.org/10.1016/j.rehab.2010.06.005

[14] Gao, X., Jie, T., Xu, D., Gál, J., Fekete, G., Liang, M., & Gu, Y. (2024). Adaptive adjustments in lower limb muscle coordination during single-leg landing tasks in Latin dancers. *Biomimetics*, *9*(8), 489. https://doi.org/10.3390/biomimetics9080489

[15] Azevedo, A. M., Oliveira, R., Vaz, J. R., & Cortes, N. (2020). Oxford foot model kinematics in landings: A comparison between professional dancers and non-dancers. *Journal of Science and Medicine in Sport*, *23*(4), 347–352. https://doi.org/10.1016/j.jsams.2019.10.018

[16] Veirs, K. P., Fagg, A. H., Haleem, A. M., Jeffries, L. M., Randall, K., Sisson, S. B., & Dionne, C. P. (2022). Applications of biomechanical foot models to evaluate dance movements using three-dimensional motion capture: A review of the literature. *Journal of Dance Medicine & Science*, *26*(2), 69–86. https://doi.org/10.12678/1089-313X.061522a

[17] Baud, R., Manzoori, A. R., Ijspeert, A., & Bouri, M. (2021). Review of control strategies for lower-limb exoskeletons to assist gait. *Journal of NeuroEngineering and Rehabilitation*, *18*(1), 119. https://doi.org/10.1186/s12984-021-00906-3

[18] Resende, R. A., Pinheiro, L. S. P., & Ocarino, J. M. (2019). Effects of foot pronation on the lower limb sagittal plane biomechanics during gait. *Gait Posture*, *68*, 130–135. https://doi.org/10.1016/j.gaitpost.2018.10.025

[19] Veirs, K. P., Rippetoe, J., Baldwin, J. D., Fagg, A., Haleem, A., Jeffries, L., . . . , & Dionne, C. P. (2023). Effects of dancer-specific biomechanics on adolescent ballet dancers' posture en pointe and factors related to pointe readiness: A cross-sectional study. *Medical Problems of Performing Artists*, *38*(3), 155–163. https://doi.org/10.21091/mppa.2023.3019

[20] Liu, Z., Zhong, Y., Chen, S., Tanaka, H., Li, Y., Katsutani, H., . . . , & Kumai, T. (2024). Effects of 4 weeks of foot exercise on subjective outcome and foot plantar pressure in elite adolescent dancers with hallux valgus: A pilot study. *BMC Sports Science, Medicine and Rehabilitation*, *16*(1), 217. https://doi.org/10.1186/s13102-024-01003-3

[21] Guo, P., Zhang, X., Xu, H., Wang, R., Li, Y., Xu, C., . . . , & Lyu, J. (2024). Evaluating plantar biomechanics while descending a single step with different heights. *Frontiers in Bioengineering and Biotechnology*, *12*, 1–14. https://doi.org/10.3389/fbioe.2024.1431988

[22] Shen, B., Zhang, S., Cui, K., Zhang, X., & Fu, W. (2022). Effects of a 12-week gait retraining program combined with foot core exercise on morphology, muscle strength, and kinematics of the arch: A randomized controlled trial. *Frontiers in Bioengineering and Biotechnology*, *10*, 1–14. https://doi.org/10.3389/fbioe.2022.1022910

[23] Wang, Y., Chen, Z., Wu, Z., Li, J., Li, C., Yang, J., & Xu, X. (2023). Reliability of foot posture index (FPI-6) for evaluating foot posture in patients with knee osteoarthritis. *Frontiers in Bioengineering and Biotechnology*, *11*, 1103644. https://doi.org/10.3389/fbioe.2023.1103644

[24] Yuan, T., Li, H., & Wang, G. (2025). Effects of kinesio taping on lower limb biomechanical characteristics during dynamic postural control tasks in individuals with chronic ankle instability. *PLoS ONE*, *20*(1), e0317357. https://doi.org/10.1371/journal.pone.0317357

[25] Abdelbar, M., Rostamjoud, F., Lára, Ármannsdóttir., Sverrisson, A., Örn., Briem, A., K, & Brynjólfsson, S. (2025). A comparative case study of EMG-driven controllers in transtibial prostheses. *IEEE Transactions on Neural Systems and Rehabilitation Engineering*, *33*, 3388–3399. https://doi.org/10.1109/tnsre.2025.3602296

[26] Aygun-Polat, E., Guzel, N. A., Guruhan, S., Polat, Y., & Karatas, N. (2025). Targeted muscle activation in Bulgarian split squat variations: Effects of trunk position and suspension-based execution. *BMC Sports Science, Medicine and Rehabilitation*, *17*(1), 251. https://doi.org/10.1186/s13102-025-01306-z

[27] Nijmeijer, E. M., Heuvelmans, P., Bolt, R., Gokeler, A., Otten, E., & Benjaminse, A. (2023). Concurrent validation of the Xsens IMU system of lower-body kinematics in jump-landing and change-of-direction tasks. *Journal of Biomechanics*, *154*, 111637. https://doi.org/10.1016/j.jbiomech.2023.111637

[28] Sturdy, J. T., Silverman, A. K., & Pickle, N. T. (2022). Automated optimization of residual reduction algorithm parameters in OpenSim. *Journal of Biomechanics*, *137*, 111087. https://doi.org/10.1016/j.jbiomech.2022.111087

[29] Nasr, A., Inkol, K. A., Bell, S., & McPhee, J. (2021). InverseMuscleNET: Alternative machine learning solution to static optimization and inverse muscle modeling. *Frontiers in Computational Neuroscience*, *15*, 759489. https://doi.org/10.3389/fncom.2021.759489

[30] Munoz-Martel, V., Santuz, A., Bohm, S., & Arampatzis, A. (2021). Proactive modulation in the spatiotemporal structure of muscle synergies minimizes reactive responses in perturbed landings. *Frontiers in Bioengineering and Biotechnology*, *9*, 761766. https://doi.org/10.3389/fbioe.2021.761766

[31] Li, X., Xu, G., Li, L., Hao, Z., Lo, W. L. A., & Wang, C. (2024). Analysis of muscle synergies and muscle network in sling exercise rehabilitation technique. *Computers in Biology and Medicine*, *183*, 109166. https://doi.org/10.1016/j.compbiomed.2024.109166

[32] Ortega-Auriol, P., Besier, T., & Mcmorland, A. J. (2025). Effect of surface electromyography normalisation methods over gait muscle synergies. *Journal of Electromyography and Kinesiology*, *80*, 102968. https://doi.org/10.1016/j.jelekin.2024.102968

[33] Russo, M., Scano, A., Brambilla, C., & d'Avella, A. (2024). SynergyAnalyzer: A Matlab toolbox implementing mixed-matrix factorization to identify kinematic-muscular synergies. *Computer Methods and Programs in Biomedicine*, *251*, 108217. https://doi.org/10.1016/j.cmpb.2024.108217

[34] Raj, E. J. S. J., & Palaniappan, R. (2024). A novel method for movement quality analysis of lower limb joints using surface electromyography signals and k-means clustering technique. *Biomedical Signal Processing and Control*, *95*, 106455. https://doi.org/10.1016/j.bspc.2024.106455

[35] Hong, X. (2021). Basketball data analysis using spark framework and K-means algorithm. *Journal of Healthcare Engineering*, *2021*(1), 6393560. https://doi.org/10.1155/2021/6393560

[36] Zhou, H., Xu, D., Quan, W., Ugbolue, U. C., Zhou, Z., & Gu, Y. (2024). Can the entire function of the foot be concentrated in the forefoot area during the running stance phase? A finite element study of different shoe soles. *Journal of Human Kinetics*, *92*, 5–17. https://doi.org/10.5114/jhk/174311

[37] Jitprapaikulsarn, S., Chantarapanich, N., Gromprasit, A., Mahaisavariya, C., Sukha, K., & Chiawchan, S. (2023). Dual plating for fixation failure of the distal femur: Finite element analysis and a clinical series. *Medical Engineering & Physics*, *111*(1), 103926. https://doi.org/10.1016/j.medengphy.2022.103926

[38] Liu, X., Yue, Y., Wu, X., Huang, X., Hao, Y., & Lu, Y. (2022). Analysis of transient response of the human foot based on the finite element method. *Technology and Health Care*, *30*(1), 79–92. https://doi.org/10.3233/thc-202673

[39] Athanasiou, K. A., Liu, G. T., Lavery, L. A., Lanctot, D. R., & Schenck, R. C. (1998). Biomechanical topography of human articular cartilage in the first metatarsophalangeal joint. *Clinical Orthopaedics and Related Research*, *348*, 269–281. https://doi.org/10.1097/00003086-199803000-00038

[40] Gefen, A. (2003). Plantar soft tissue loading under the medial metatarsals in the standing diabetic foot. *Medical Engineering & Physics*, *25*(6), 491–499. https://doi.org/10.1016/s1350-4533(03)00029-8

[41] Wong, D. W.-C., Niu, W., Wang, Y., & Zhang, M. (2016). Finite element analysis of foot and ankle impact injury: Risk evaluation of calcaneus and talus fracture. *PLoS ONE*, *11*(4), e0154435. https://doi.org/10.1371/journal.pone.0154435

[42] Chvatal, S. A., & Ting, L. H. (2013). Common muscle synergies for balance and walking. *Frontiers in Computational Neuroscience*, *7*, 48. https://doi.org/10.3389/fncom.2013.00048

[43] Hug, F., Turpin, N. A., Couturier, A., & Dorel, S. (2011). Consistency of muscle synergies during pedaling across different mechanical constraints. *Journal of Neurophysiology*, *106*(1), 91–103. https://doi.org/10.1152/jn.01096.2010

[44] Giakas, G., & Baltzopoulos, V. (1997). Time and frequency domain analysis of ground reaction forces during walking: An investigation of variability and symmetry. *Gait & Posture*, *5*(3), 189–197. https://doi.org/10.1016/s0966-6362(96)01083-1

[45] Fong, C.-M., Blackburn, J. T., Norcross, M. F., McGrath, M., & Padua, D. A. (2011). Ankle-dorsiflexion range of motion and landing biomechanics. *Journal of Athletic Training*, *46*(1), 5–10. https://doi.org/10.4085/1062-6050-46.1.5

[46] Mattiussi, A. M., Shaw, J. W., Price, P., Brown, D. D., Cohen, D. D., Lineham, J., . . . , & Atack, A. (2024). The association of range of motion, lower limb strength, and load during jump landings in professional ballet dancers. *Journal of Biomechanics*, *168*, 112119. https://doi.org/10.1016/j.jbiomech.2024.112119

[47] Foster, A. D., Block, B., Capobianco, III., Peabody, F., T, J., Puleo, N. A., . . . , & Vegas, A. (2021). Shorter heels are linked with greater elastic energy storage in the Achilles tendon. *Scientific Reports*, *11*(1), 9360. https://doi.org/10.1038/s41598-021-88774-8

[48] Toussaint, T. D., & Schepens, B. (2024). Biomechanical behavior of the lower limbs and of the joints when landing from different heights. *Journal of biomechanics*, *165*, 112014. https://doi.org/10.1016/j.jbiomech.2024.112014

[49] Koh, K., Park, Y. S., Park, D. W., & Shim, J. K. (2020). Dance training improves the CNS's ability to utilize the redundant degrees of freedom of the whole body. *Scientific Reports*, *10*(1), 22197. https://doi.org/10.1038/s41598-020-79081-9

[50] Akuzawa, H., Morito, T., Oshikawa, T., Kumai, T., & Kaneoka, K. (2023). Functional relationship between the foot intrinsic and extrinsic muscles in walking. *Journal of Electromyography and Kinesiology*, *71*, 102781. https://doi.org/10.1016/j.jelekin.2023.102781

[51] Ogawa, Y., Maemichi, T., Yamaguchi, R., Okunuki, T., Kinoshita, O., Nagamoto, H., & Kumai, T. (2024). Differences in muscle activity of extrinsic and intrinsic foot muscles in toe grip and push-down movements of the great toe. *The Foot*, *60*, 102111. https://doi.org/10.1016/j.foot.2024.102111

[52] Ellison, M. A., Fulford, J., Javadi, A., & Rice, H. M. (2021). Do non-rearfoot runners experience greater second metatarsal stresses than rearfoot runners? *Journal of Biomechanics*, *126*, 110647. https://doi.org/10.1016/j.jbiomech.2021.110647

[53] Lei, Y., Wang, Q., Tang, J., & Kang, P. (2025). Dance-related injuries: An evidence-based review of epidemiology, mechanisms, and prevention strategies. *Current Physical Medicine and Rehabilitation Reports*, *13*(1), 49. https://doi.org/10.1007/s40141-025-00523-4

[54] Iafrate, J. L., Townsend, C. E., Scott, C., Yun, H. J., Ventola, A., & Semanson, S. (2021). Diagnosis and management of foot and ankle injuries in dancers. *Current Physical Medicine and Rehabilitation Reports*, *9*(3), 47–56. https://doi.org/10.1007/s40141-021-00313-8

[55] Katakura, M., Kedgley, A. E., Shaw, J. W., Mattiussi, A. M., Kelly, S., Clark, R., . . . , & Calder, J. D. (2023). Epidemiological characteristics of foot and ankle injuries in 2 professional ballet companies: A 3-season cohort study of 588 medical attention injuries and 255 time-loss injuries. *Orthopaedic Journal of Sports Medicine*, *11*(2), 23259671221134131. https://doi.org/10.1177/23259671221134131

[56] Buckley, R., Ellison, M., & Dixon, S. (2025). The effects of forefoot bending stiffness in athletic footwear on stresses in the second metatarsal. *Footwear Science*, *17*(S1), S283–S284. https://doi.org/10.1080/19424280.2025.2492284

[57] Farhadi, F. (2026). Extended finite element analysis for the 2nd and 3nd metatarsals stress fracture during push-off. *Computer Methods in Biomechanics and Biomedical Engineering*, *29*(1), 12–22. https://doi.org/10.1080/10255842.2024.2374528

How to Cite: Gao, X., Xu, D., Liang, M., Zhang, Z., Jie, T., Zhou, H., …, & Gu, Y. (2026). Adaptive Mechanisms of Foot Function and Control Induced by Dance Training. *Artificial Intelligence and Applications*. https://doi.org/10.47852/bonviewAIA62028273